



Microporous activated carbons from coconut shells produced by self-activation using the pyrolysis gases produced from them, that have an excellent electric double layer performance

Kang Sun^{1,2}, Chang-yu Leng¹, Jian-chun Jiang^{1,2,*}, Quan Bu³, Guan-feng Lin⁴, Xin-cheng Lu¹, Guang-zhen Zhu¹

¹Institute of Chemical Industry of Forest Products, Chinese Academy of Forestry, Nanjing 210042, China;

²Research Institute of Forestry New Technology of Forestry, Chinese Academy of Forestry, Beijing 100091, China;

³School of Agricultural Equipment Engineering, Jiangsu University, Zhenjiang 212013, China;

⁴Jinshan College of Fujian Agriculture and Forestry University, Fuzhou 350002, China

Abstract: Coconut shell-based activated carbons were prepared by self-activation using the pyrolysis gases generated from them. The process was carried out at high temperatures in a closed reactor filled with coconut shell under a high pressure that was generated by pyrolysis gases. Results indicate that the activated carbon prepared at 900 °C for 6h has a specific surface area, total pore volume, micropore percentage, iodine adsorption capacity and methylene blue adsorption capacity of 1 194.4 m²/g, 0.528 cm³/g, 87.8%, 1 280 mg/g and 315 mg/g, respectively. When used as the electrode material of electrochemical capacitors this activated carbon exhibits a specific capacitance of 258 F/g, a high capacitance retention rate of 97.2% after 3000 charge/discharge cycles and a small impedance. The water vapor and carbon dioxide generated by the pyrolysis of the coconut shell in the closed reactor act as activating agents and also increase the pressure of the reaction system. This is favorable for the activation of the formed char. This self-activation method was also used to prepare activated carbons with high adsorption capacities for iodine and methylene blue from almond stones, pecan shells and slash pine sawdust, indicating that it is a very simple, efficient, environmentally friendly and economical method for the preparation of biomass-based activated carbons for supercapacitor electrode materials and adsorption.

Key Words: Activated carbons; Porous structure; Thermochemical activation; Alkali activation; Supercapaci

1 Introduction

Biomass is the most abundant reserves of renewable organic resources on the Earth, which is cheap and easy available. Because it is rich in cellulose, semi cellulose, lignin, and low in inorganic impurities, biomass is the particularly promising raw material for preparation of activated carbons (ACs).

For example, a wide variety of biomass materials, including lignin, walnut and coconut shells, coffee beans, firewood, bamboo, rice husk, animal bones, animal feather, fungi, tea leaves, cocoon, dead leaves, banana peel and sugarcane bagasse, have been used as the raw materials for the preparation of ACs.

ACs are prepared mainly by physical and chemical activation. The physical activation of carbonized biomass consumes about 5 tons of water vapor or carbon dioxide per

ton of feed, and a large amount of heat is required to heat water or carbon dioxide. This process is complex and the yield is lower than 10% [1]. The chemical activation of biomass with H₃PO₄ [2], ZnCl₂ [3], or KOH [4] consumes chemical weight 4-6 times as much as feed. Moreover, the ACs prepared by chemical activation have a high content of metal impurities generally above 3000 mg/kg, which can block some pores of ACs, leading to a high self-discharge of AC electrode and a short cycle life of supercapacitors. In order to remove those chemical impurities from ACs, a large amount of deionized water is needed to wash the ACs after chemical activation, generating a large quantity of waste water. What is more, gas pollutants are also released during the chemical activation.

In order to reduce pollutants, a kind of environment friendly activation method is urgently needed to activate carbons. In the present study, a self-activation with pyrolysis gases (PSAM) was first employed to prepare microporous

activated carbon using biomass as feed without aid of any physical or chemical agent. The activation was carried out in a covered reactor, in which a gas mixture from biomass pyrolysis was used as activation agents to create micropores in the biochar under an autogenerated pressure that can accelerate the activation rate [5, 6]. In this method, the air enclosed in the reactor and the oxygen adsorbed by the biomass feed can also act as activation agents [7].

Supercapacitors (SCs), also known as electrochemical capacitors, have recently gained much attention owing to its high power density and long cycle life [8,9]. On the basis of the charge storage mechanisms, supercapacitors have two categories, electrical double layer capacitors (EDLCs) and pseudocapacitor^[10-11]. The capacitance for EDLC originates from pure electrostatic charge separation at the interface between electrode and electrolytes, which requires electrode materials with a large specific surface area and well-developed pores [12]. Up to now, a variety of carbon-based materials such as ACs, carbon aerogels, carbon nanotubes, carbon nanofibers, and graphene have been utilized as the electrode materials for EDLCs^[13-15]. Among them, ACs are considered as one of the most attractive candidates for EDLCs because of its large surface area, developed microporous structure, excellent chemical stability and low cost^[16-18].

In this study, the EDLC capacitance of ACs prepared by the self-activation of biomass with pyrolysis gases as the electrode of EDLCs was determined. The effects of reaction conditions including the moisture content, reaction time and reaction temperature on the properties of the ACs were investigated. The activation mechanism of this method was analyzed.

2. Experimental

2.1 Preparation

Coconut shell, almond stone, pecan shell and slash pine sawdust were selected as feeds, and the AC samples prepared with these feeds were labeled as CSAC, ASAC, PSAC, SPAC, respectively. The elemental and proximate analysis of the feeds are summarized in Table 1. A stainless steel autoclave was used to maintain autogenerated pressure in the self-activation as shown Fig.1. The raw materials were pre-crushed to smaller than 1mm, washed with deionized water and dried under 150 °C for 2 h. Then, they were put into the autoclave reactor, keeping their volume not exceed 1/3 of the reactor volume. Then the reactor was sealed and put in a quartz tube furnace. The temperature was increased to 700-1000 °C at a heating rate of 5 °C/min. The samples were held at the targeted temperature for 2-8 h. Finally, the products were collected from the reactor after it was cooled to room temperature. During the activation, a large number of pyrolysis gases were generated, which can generate certain autogenerated pressure under high temperature. So the reactor was always kept sealed during the activation.

2.2 Characterizations

Nitrogen adsorption isotherm was measured by a Micromeritics ASAP2020 absorption analyzer at 77 K. Before analysis, the samples were degassed at 200 °C for 24 h. The surface area was calculated according to the Brunauer-Emmett-Teller (B.E.T) method. Pore size distribution was calculated based on the density function theory (DFT) method from nitrogen adsorption data by assuming a slit pore geometry. Scanning electron microscopic (SEM) analysis was conducted by a S-3400-SEM (Toshiba). Before observation, E-1010 ion-covered plane was used to spray metal on materials. Transmission electron microscopic (TEM) investigations were performed on a FEI Tecnai G2 T20 microscope operated at 200 kV. XRD analysis was performed with a PANalytical X'Pert Pro MPD diffraktometer using Cu Ka-Radiation (40 kV, 40 mA). Scanning resolution was 0.02-2h and 1s per step. Thermo-gravimetric analysis (TG) was carried out by a DSC -TG STA 409 (Netzsch, German). 1 g sample, under the protection of the nitrogen flow, was put into the DSC/ -TG and the temperature was raised to 900 °C with a heating rate of 10 °C/min and maintained for 10 min. The composition of pyrolysis gases was analyzed by GC/MS of a QMS 403C (NETZSCH Company, Germany). With a heating rate of 10 K/min, an outlet temperature of 220 °C, the ion current intensity of mass-to-charge ratios for the pyrolysis gases were continuously detected. The gas composition was inferred according to characteristic peaks of various substances. The gaseous components were qualitatively determined by comparing with a relevant standard gas, and quantitatively determined using a single point external standard.

2.3 Electrode preparation and electrochemical measurements

The EDLC performance of all samples was evaluated at room temperature using a double electrode system. The working electrodes were prepared by mixing 85 wt% microporous carbon, 10 wt% carbon-black, and 5 wt% polytetrafluoroethylene, and rolling into a thin film. After being pressed, the film was cut into disks of 11mm in diameter with an approximate mass load of 6 mg/cm². 1M H₂SO₄ was used as an electrolyte. Galvanostatic charge-discharge (GCD) experiments were conducted with a VMP3B-2x2, Bio-Logic electrochemical workstation.

The specific capacitance of the electrode material was

derived according to $C = \frac{2I}{(dV/dt)m}$ where I is the current

(A), dV/dt is the slope of discharge curve (V·s⁻¹), and m is the mass (g) of the active material in each electrode.

Table 1 Elemental and proximate analysis of feeds

Sample	Element					* Proximate			
	C carbon	H hydrogen	O oxygen	N nitrogen	S sulfur	moisture	ash	volatile	fixed carbon
Coconut	49.14	6.37	42.47	0.13	0.71	13.26	0.76	77.70	21.54
Almond stone	48.76	7.52	43.68	0.48	0.56	11.05	2.11	77.32	20.57
Pecan shell	48.65	6.69	44.11	0.42	0.13	10.16	1.58	78.63	19.79
Slash pine sawdust	47.6	6.45	45.40	0.55	0.21	7.89	3.42	76.11	20.47

Note: * ash, volatile and fixed carbon based on dry feed.

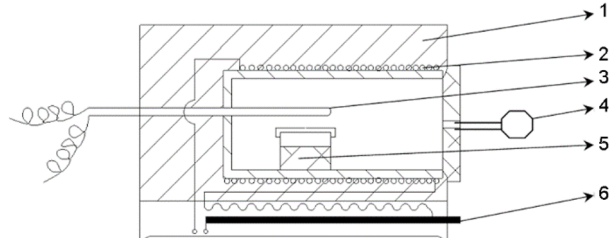


Fig. 1 Schematic diagram of the self - activation device with pyrolysis gases (1. furnace, 2. resistance wire, 3. thermocouple, 4. pressure gauge, 5. stainless steel autoclave reactor, 6. electric heating rod)

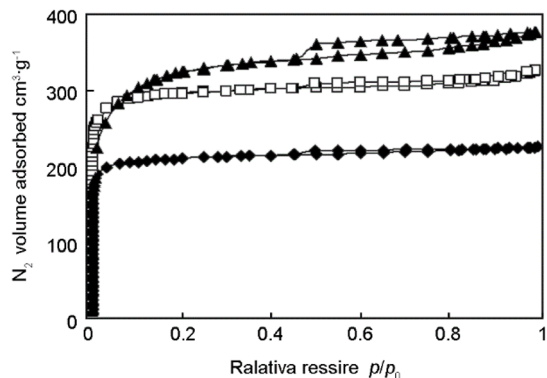


Fig.2 N₂ adsorption isotherms of CSACs prepared at different activation temperatures (▲1000 °C; □900°C; ◆800° Cadorption)

3 Results and discussion

3.1 N₂ adsorption

Pyrolysis/self-activation temperature and holding time had a great impact on the pore structures of CSACs. As shown in Fig. 2, the three adsorption isotherms exhibited curves closed to a Type I isotherm according to the IUPAC classification. The N₂ uptake increased sharply at low relative pressures (p/p_0) from 0 to 0.1, but leveled off at the high relative pressures from 0.1 to 0.99, which implied that CSACs had a developed microporous structure. The three adsorption isotherms up-shifted gradually as the activation temperature increased from 800 to 1000 °C, indicating that their total pore volume increased gradually. The sample prepared at 900 °C had no obvious hysteric loop in the adsorption-desorption isotherm, indicating it had only a small number of mesopores. When the activation temperature was increased to 1000 °C, the isotherms showed an obvious hysteric loop, which indicated that there was a moderate number of mesopores. It

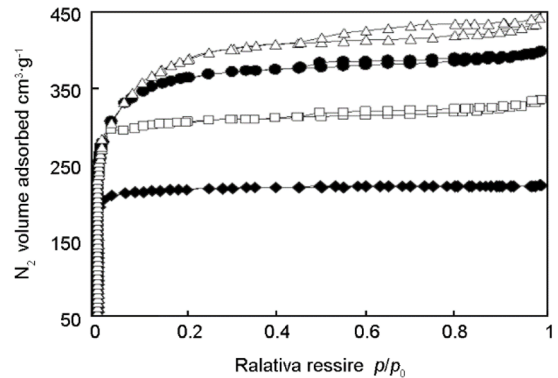


Fig.3 N₂ adsorption isotherms of CSACs at different activation times (△8h; ●6h; □4h; ◆2h)

revealed that partial micropore walls collapsed under a high activation temperature, leading to a decrease of the microporosity and an increase of the mesoporosity.

Fig. 3 represents the N₂ adsorption isotherms of the CSACs prepared at different activation times. All the samples gave a Type I isotherm according to the IUPAC classification. The curves up-shifted gradually with the activation time. It was obviously observed that the lowest isotherm was achieved at an activation time of 2 h. This demonstrated that the total pore volume was the smallest because the activation had not been performed insufficiently. When the activation time was increased to 6 h, N₂ adsorption volume increased rapidly at the relative pressures below 0.2, but leveled off at the relative pressures from 0.2 to 0.99. But the hysteresis loop is not clear, indicated that few meso- and macro-pores existed in the activated carbon. When the activation time was increased further to 8 h, an obvious hysteresis loop was observed, suggesting that some of the micropores were widened with the generation of mesopores and the decrease of micropore percentage.

Table 2 Characteristics of pore structure of CSACs

Temp. ^a (°C)	Time (h)	S _{B.E.T.} ^b (m ² ·g ⁻¹)	V _t ^c (cm ³ ·g ⁻¹)	V _{micro} ^c (cm ³ ·g ⁻¹)	R _{micro} ^d (%)	V _{meso} ^c (cm ³ ·g ⁻¹)	R _{meso} ^d (%)	D ^e (nm)
800	6	803	0.345	0.297	86.10	0.031	9.20	1.98
900	6	1194	0.528	0.446	87.80	0.071	13.40	2.02
1000	6	1149	0.558	0.405	72.50	0.118	21.20	2.12
900	2	717	0.334	0.291	87.10	0.028	9.10	1.94
900	4	942	0.569	0.449	78.90	0.089	15.60	2.05
900	8	1087	0.607	0.428	70.50	0.136	22.50	2.14

Note: a: Activation temperature; b: Specific surface area calculated by Brunauer -Emmett-Teller method; c: Total, micro- and meso- pore volume from N₂ adsorption; d: Ratio of micropore and mesopore; e: Average pore size.

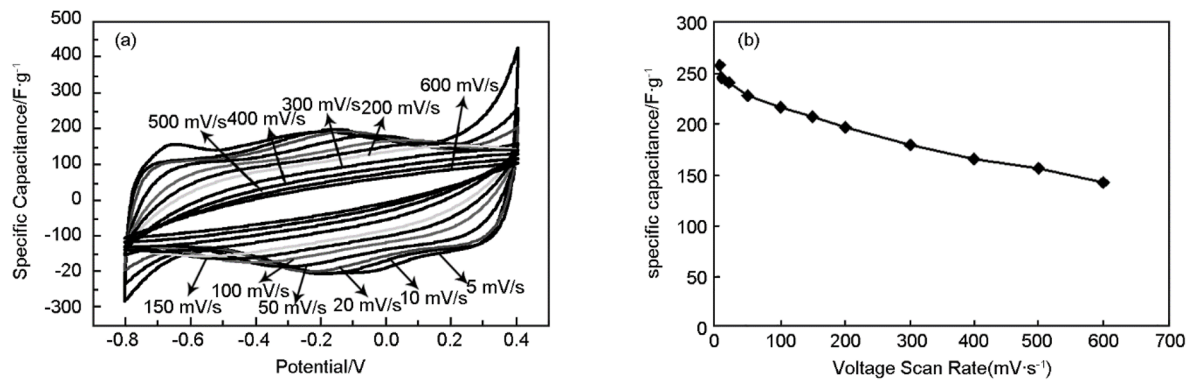


Fig. 4 Effect of cyclic voltammograms (CV) and scanning speed on specific capacitance, (a) CV measurements of the CSAC electrode at different scan rates; (b) specific capacitance calculated from the CV measurements at various scan rate

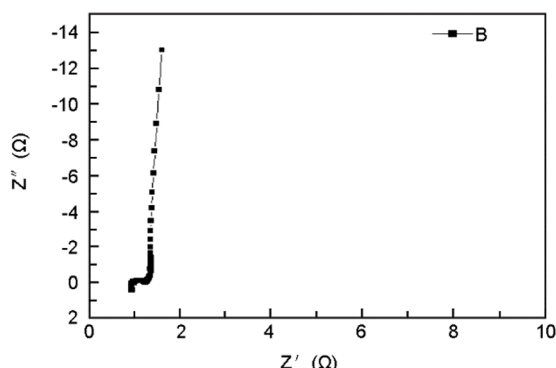


Fig. 5 Nyquist plot for the CSAC electrode

3.2 Specific surface area and pore structure

Table 2 summarizes the pore characteristics of the CSACs. The specific surface area and total pore volume increased with the activation temperature and activation time. The ratio of micropores reached 87.80% at 900 °C, but decreased slightly with the temperature up to 1000 °C. The average pore diameter was increased with the activation temperature. The effect of activation time on the pore structure is the same as that of the activation temperature. This phenomenon is due to the fact that which micropores were generated firstly, and developed to mesopores and macropores with the proceeding of the self-activation. Under high temperature, partial micropores were enlarged while new micropores were generated. When the widening speed of micropores exceeded the generation speed of new micropores, the number of

mesopores and macropores increased while the number of micropores decreased. Hence, the activated carbon with a high microporosity (HMAC) could be prepared by controlling the activation temperature and activation time carefully in the self-activation with pyrolysis gases.

3.3 EDLC performance

The CSAC with the highest micropore ratio prepared in this work was selected as the electrode material of EDLC. The cyclic voltammograms and the effect of scanning speed on specific capacitance are shown in Fig. 4. EDLC performance of the CSAC was evaluated with a two-electrode system using 1 M H₂SO₄ as the electrolyte. According to the equation (1), the specific capacitance of the CSAC was calculated as 258 F/g. As shown in Fig. 3a, the capacitance is higher at a lower scanning speed, which indicated that the CSAC had rich micropores. The cyclic voltammetry curve can still maintain the rectangular shape, even at a very high scanning speed of 600 mV/s, which shows that the CSAC has a much better capacitance performance.

The electrochemical impedance spectra (EIS) of the CSAC is shown in Fig. 5. The plot exhibited a semicircle in the high-frequency region and a straight line in the low-frequency region [19]. The small semicircle in the high-frequency region indicates a very low charge transfer resistance. This is due to its pore structure, in which the micropores were internally connected with each other. The interconnected pore structure facilitated the rapid diffusion of electrolyte ions into the micropores of the electrode material.

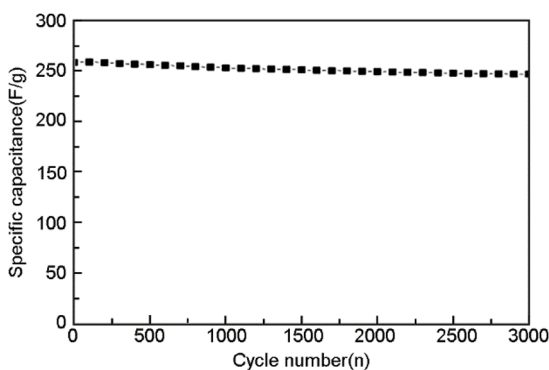


Fig.6 The cycling performance of the CSAC at a current density of 1 $A \cdot g^{-1}$

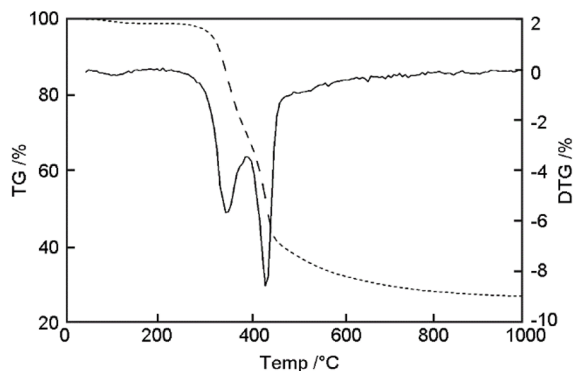


Fig. 7 TG-DTG curves of coconut shell

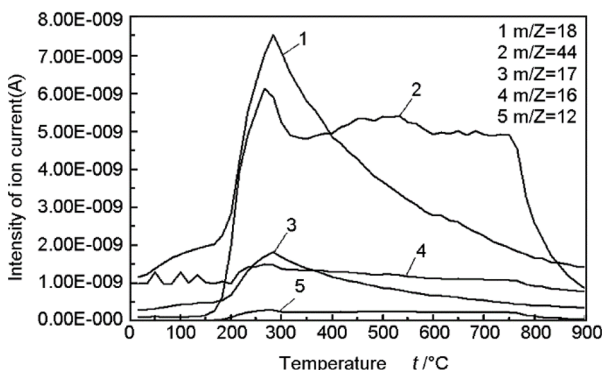


Fig. 8 GC/MS curves of the pyrolysis gases of coconut shell

In addition, the plot showed a vertical line to the imaginary axis in the low-frequency region, suggesting that the CSAC had a good capacitive behavior^[20].

Fig. 6 shows the cyclic performance of the CSAC. It can be seen that the CSAC had a long charge-discharge cycle life, since its discharge capacitance was kept at 97.2% of the maximum discharge capacity after 3000 cycles. That is due to the self-activation method proposed in this paper that does not use any chemical agents, avoiding contamination of the materials, which can keep clear of pore channels. Therefore, the CSAC prepared by self-activation is suitable for the electrode material of EDLCs.

3.4 Mechanism of activation

3.4.1 Micropores created by pyrolysis gases

Fig. 7 shows the TG-DTG curve of coconut shell. At the temperature below 200 °C, a small amount weight loss is related to dehydration of coconut shell. The main weight loss of 70% took place in the most intense pyrolysis temperature between 200 and 500 °C, which was accompanied by releasing a large number of pyrolysis gases from coconut shell. The semi-cellulose that is the most unstable part of the woody materials decomposed between 225 and 325 °C, the cellulose between 300 and 375 °C, and the lignin between 250 and 500 °C^[21]. As the pyrolysis temperature was elevated from 500 to 1000 °C, all the pyrolysis gases were released and about 30 wt% solid char was left.

The components of the gas mixture produced at different pyrolysis temperatures from coconut shell were detected by mass spectrometry. It can be seen from the peaks in Fig. 8 that the pyrolysis gases are mainly H₂O (m/z=17, 18), CO₂ (m/z=44) and CH₄/C₂H₆ (m/z=12, 16). The CO₂ and H₂O, a large portion of gases, are good activation agents, which evolved above 300 °C. The results indicated that the excellent activation atmosphere could be generated in the covered reactor, which can activate the char to create micropores in the self-activation^[22-27].

Fig. 9 illustrates the mechanism of pore formation in the self-activation with pyrolysis gases, which include two steps. As shown in Fig. 9a, the first step happened in the temperature range of 200-500 °C, in which a large volume of pyrolysis gases escaping from coconut shell generates channel. Fig. 9b exhibits the second step happened in the high temperature range of 800-1000 °C, during which a high pressure is produced in the sealed reactor. The pyrolysis gases were forced into the channel of solid char under the autogenerated pressure and created micropores by gasification reactions with carbon. At the same time, the high pressure can also promote the gasification reaction rate^[28] to develop micropores in the self-activation with pyrolysis gases.

3.4.2 The self-activation promoted by autogenerated pressure

In order to measure the autogenerated pressure in the sealed system, a high-temperature-proof pressure gauge was installed at the top of the tube furnace. The system pressure was recorded when temperature was increased to 600, 700, 800, 900 and 1000 °C at a heating rate of 10 °C/min. Pressure gauge read was a constant value when the temperature was kept unchanged. Fig. 10 exhibits the relationship of autogenerated pressure and temperature in the sealed reactor. It can be seen that the autogenerated pressure increased with the temperature because the pyrolysis gases were expanded to increase pressure in the sealed reactor under a high temperature.

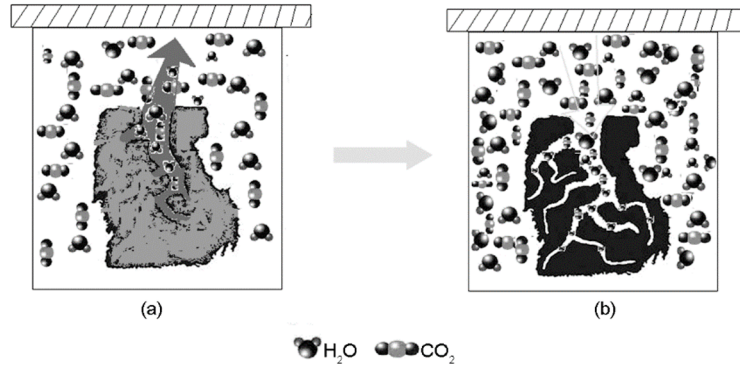


Fig. 9 An illustration of self-activation mechanism that creates micropores (a) channel formed by escaping pyrolysis gases between 200 and 500 °C and (b) micropores created by pyrolysis gases in the solid char at 800-1000 °C.

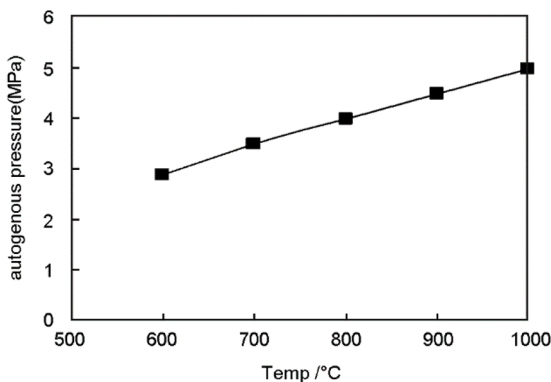


Fig. 10 Relationship of autogenerated pressure

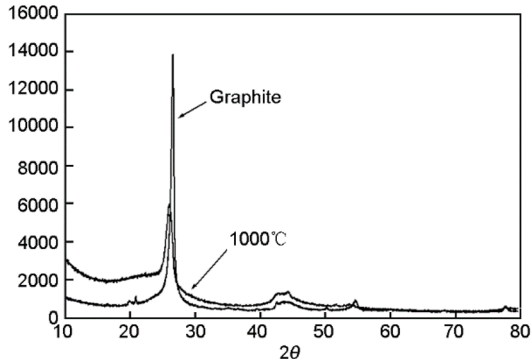


Fig. 11 XRD patterns of the CSAC and natural graphite

3.4.3 Carbon crystallite and its evolution

Fig. 11 exhibits the XRD patterns of the CSAC and natural graphite. The XRD diffraction pattern of the CSAC showed two peaks at 23° and 44°, which corresponded to graphite crystallites. Compared with the XRD pattern of natural graphite, the diffraction peaks of the CSAC slightly shifted to the small diffraction angle direction, indicating that the d-space of carbon layer of the CSAC is larger than that of natural graphite. The d-space of the CSAC was calculated to be 0.42 nm, which is larger than 0.34 nm of the ideal graphite. Because the carbon microcrystallite derived from biomass is disorder and instable, it becomes ordered under high temperature and high pressure. The carbon layer tends to be regular, making mesopore shrink to form new micropores, which leads to the increase of microporosity and electric

conductivity^[29].

Fig. 12 shows the TEM image of the CSAC prepared with the self-activation with pyrolysis gases at 900 °C. Fig. 12a shows a TEM picture of channel and pore of the CSAC. The sample has a very novel pore structure like a tree root, which is shown in supporting information in Fig.8. The channel formed by escaping pyrolysis gases and the micropores generated by gas activation were significant, and both type connected with each other. The interconnected porosity is in favor of the electrolyte ion access to the huge internal area of the CSAC, which is very important for the electrode materials of supercapacitors.

Fig. 12b is a high resolution TEM picture, showing rich micropores and surface of the CSAC. Fig. 12c shows the image of the yellow region 1 of Fig. 12b, which further revealed that the CSAC had a highly porous structure with a large percentage of micropores. Fig.12d shows the image of the yellow region 2 of Fig.12b, indicating that the surface of the CASC was covered obviously with a graphite layer about 24 graphene sheets. This indicated that coconut shell could be transformed into the graphite like structure under high temperature and pressure, a which is in consistent with the analysis results from XRD. The improvement of the conductivity of the CSAC by the graphite like structure is surely beneficial to improve the electrochemical performance of supercapacitors^[30].

3.5 Applicability of the self-activation method in other raw materials

In order to determine the applicability of the self-activation with pyrolysis gases in the other raw materials, almond stone, pecan shell and slash pine sawdust were also selected as feeds to prepare ACs with an activation temperature 900 °C and a holding time 6 h. The yield and adsorption properties are given and compared as shown in Table 3. It was observed from Table 2 that ACs can all be prepared with the self-activation with pyrolysis gases from the selected three feeds. The samples had good adsorption capacities for iodine and methylene blue of 972-1200 mg·g⁻¹ and 180-315 mg·g⁻¹, respectively. Besides, the coconut shell was obviously the best among them.

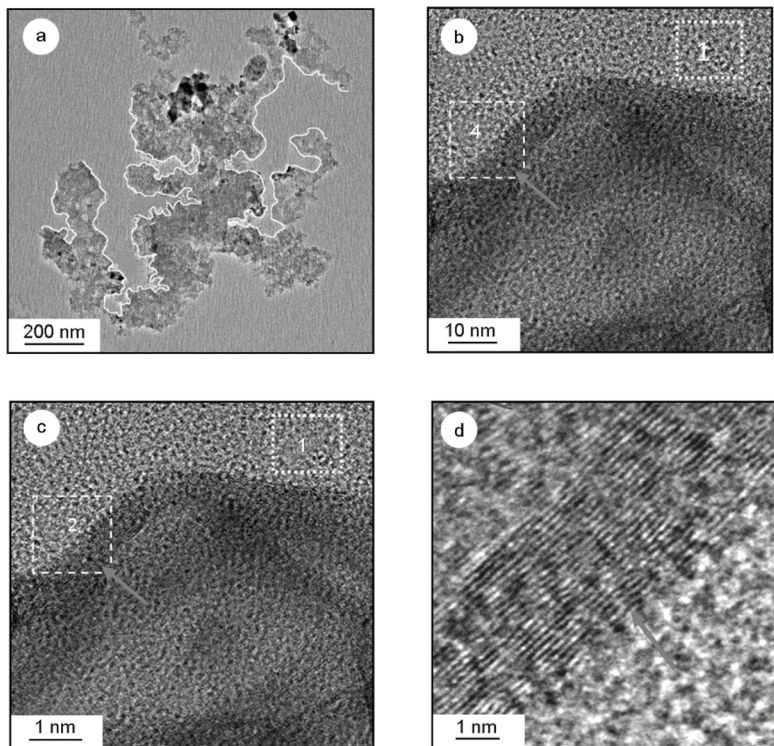


Fig.12 TEM images of the CSAC prepared by the self-activation at 900 °C

Table 3 Results of activated carbons prepared by the self-activation with pyrolysis gases

Feed	Temperature /°C	Time /h	yield /%	MB capacity (mg·g⁻¹)	I_2 capacity (mg·g⁻¹)
Coconut shell	900	6	13.8	315	1280
Almond stone	900	6	12.4	180	1119
Pecan shell	900	6	12.5	255	972
Slash pine sawdust	900	6	5.7	240	1028

Note: MB capacity: methylene blue adsorption capacity. I_2 capacity: iodine adsorption capacity.

4 Conclusions

The self-activation with pyrolysis gases was firstly developed to prepare high microporous biomass-based ACs without using any activation agent. The obtained coconut shell based activated carbon showed a micropore ratio of 87.7% and a specific capacitance of 258 F/g. Because the micropore structure was formed as a conductive network, the activated carbon had a very small impedance and kept 97.2% of initial capacitance after 3000 charge/discharge cycles. The high temperature and autogenerated pressure made it possible to transform disordered carbon to graphite structure on the surface of coconut shell activated carbon, which improved the conductivity of the material. While no chemical agent was used, the activated carbon was pure and suitable for the electrode of super capacitor. The almond stone, walnut shell and slash pine sawdust were also selected as feeds to verify the effectiveness of the self-activation with pyrolysis gases, and results indicated that the prepared activated carbons showed a good adsorption capacity for iodine and methylene

blue. This work reveals the activation mechanism of the self-activation with pyrolysis gases, which will contribute to the development of a very simple, efficient, environmental friendly and economical process for the preparation of biomass-based ACs for super capacitor electrode materials and adsorption materials.

Acknowledgments

This research is financially supported by the projects in forestry public benefit research sector (201404610), and the national natural science foundation of China (31400510).

References

- [1] Qiang L, Yin W, Jian Y, et al. Preparation and characterization of activated carbons from spirit lees by physical activation[J]. Carbon, 2012, 55(1): 376.
- [2] Jagtoyen M, Derbyshire F. Activated carbons from yellow and white oak by H_3PO_4 activation[J]. Carbon, 1998, 36(7-8): 1085-1097.

- [3] Caturla F, Molina-Sabio M, Rodríguez-Reinoso F. Preparation of activated carbon by chemical activation with $ZnCl_2$ [J]. *Carbon*, 1991, 29(7): 999-1007.
- [4] Elmouwahidi A, Zapata-Benabithe Z, Carrasco-Marín F, et al. Activated carbons from KOH-activation of argan (*Argania spinosa*) seed shells as supercapacitor electrodes[J]. *Bioresource Technology*, 2012, 111(1): 185-190.
- [5] Pol S V, Pol V G, Gedanken A. Reactions under autogenerated pressure at elevated temperature (RAPET) of various alkoxides: formation of metals/metal oxides-carbon core-hell structures[J]. *Chemistry*, 2004, 10(18): 4467-473;
- [6] Gershi H, Gedanken A, Keppner H, et al. One-step synthesis of prolate spheroidal-shaped carbon produced by the thermolysis of octene under its autogenerated pressure[J]. *Carbon*, 2011, 49(4): 1067-1074.
- [7] Man S T, Antal M J. Preparation of activated carbons from macadamia nut shell and coconut shell by air activation [J]. *Industrial & Engineering Chemistry Research*, 1999, 38(11): 4268-4276.
- [8] Qu W H, Xu Y Y, Lu A H. Converting biowaste corncob residue into high value added porous carbon for supercapacitor electrodes[J]. *Bioresource Technology*, 2015, 189:285-291.
- [9] Doyle M D, Loushine RJ, Agee K A, et al. Preparation of highly porous binderless activated carbon electrodes from fibres of oil palm empty fruit bunches for application in supercapacitors.[J]. *Journal of Endodontics*, 2013, 39(3): 254-261.
- [10] Nishihara H, Itoi H, Kogure T, et al. Investigation of the ion storage/transfer behavior in an electrical double-layer capacitor by using ordered microporous carbons as model materials[J]. *Chemistry*, 2009, 15(15): 5355-5363.
- [11] Ma G, Qian Y, Sun K. Nitrogen-doped porous carbon derived from biomass waste for high-performance supercapacitor[J]. *Bioresource Technology*, 2015, 197: 137-142.
- [12] Kötz R, Carlen M. Principles and applications of electrochemical capacitors[J]. *Electrochimica Acta*, 2000, 45(s 15-16): 2483-2498.
- [13] Fang B, Binder L. A modified activated carbon aerogel for high-energy storage in electric double layer capacitors[J]. *Journal of Power Sources*, 2006, 163(1): 616-622.
- [14] Zhu Y, Murali S, Cai W, S et al. Graphene and graphene oxide: synthesis, properties, and applications[J]. *Advanced Materials*, 2010, 22(35): 3906-3924.
- [15] Jiang W, Zhai S, Wei L. Nickel hydroxide–carbon nanotube nanocomposites as supercapacitor electrodes: crystallinity dependent performances[J]. *Nanotechnology*, 2015, 26(31).
- [16] Yu H R, Cho S, Jung M J. Electrochemical and structural characteristics of activated carbon-based electrodes modified via phosphoric acid[J]. *Microporous & Mesoporous Materials*, 2013, 172(172): 131-135.
- [17] Redondo E, Carretero-González J, Goikolea E. Effect of pore texture on performance of activated carbon supercapacitor electrodes derived from olive pits[J]. *Electrochimica Acta*, 2015, 160:178-184.
- [18] Qu D. Studies of the activated carbons used in double-layer supercapacitors[J]. *Journal of Power Sources*, 2002, 109(2): 403-411.
- [19] Chang J, Gao Z, Wang X. Activated porous carbon prepared from paulownia flower for high performance supercapacitor electrodes[J]. *Electrochimica Acta*, 2015, 157: 290-298.
- [20] Oh I, Kim M, Kim J. Deposition of Fe_3O_4 on oxidized activated carbon by hydrazine reducing method for high performance supercapacitor[J]. *Microelectronics Reliability*, 2015, 55(1): 114-122.
- [21] Sundaram E G, Natarajan E. Department. Pyrolysis of coconut shell: an experimental investigation[J]. 2009, 6(2): 33-39
- [22] Rodríguez-Reinoso F, Molina-Sabio M, González M T. The use of steam and CO_2 as activating agents in the preparation of activated carbons[J]. *Carbon*, 1995, 33(1): 15-23.
- [23] Xing J, Xia S, Dong K. Preparation and characterization of activated carbon from acorn shell by physical activation with H_2O-CO_2 in two-step pretreatment[J]. *Bioresource Technology*, 2013, 136 (4): 163-168.
- [24] Shim T, Yoo J, Ryu C. Effect of steam activation of biochar produced from a giant Miscanthus on copper sorption and toxicity[J]. *Bioresource Technology*, 2015, 197: 85-90.
- [25] Rodríguez-Valero M A, Martínez-Escandell M, Molina-Sabio M. CO_2 activation of olive stones carbonized under pressure[J]. *Carbon*, 2001, 39(2): 320-323.
- [26] Lahijani P, Zainal Z A, Mohamed A R. Microwave-enhanced CO_2 gasification of oil palm shell char[J]. *Bioresource Technology*, 2014, 158(2): 193-200.
- [27] Roberts D G, Harris D J. Char gasification with O_2 , CO_2 , and H_2O : Effects of pressure on intrinsic reaction kinetics[J]. *Energy Fuels*, 2000, 14(2): 483-489.
- [28] Seebauer V, Petek J, Staudinger G. Effects of particle size, heating rate and pressure on measurement of pyrolysis kinetics by thermogravimetric analysis[J]. *Fuel*, 1997, 76(13): 1277-1282.
- [29] Jiang L, Yan J, Hao L, et al. High rate performance activated carbons prepared from ginkgo shells for electrochemical supercapacitors[J]. *Carbon*, 2013, 56(56): 146-154.
- [30] Sánchez-González J, Stoeckli F, Centeno T A. The role of the electric conductivity of carbons in the electrochemical capacitor performance[J]. *Journal of Electroanalytical Chemistry*, 2011, 657(657): 176-180.